J Mater Sci: Mater Med (2010) 21:2141–2149
DOI 10.1007/s10856-010-4068-7

Nanosilicon carbide/hydroxyapatite nanocomposites: structural, mechanical and in vitro cellular properties

Saeed Hesaraki · Touraj Ebadzadeh · Shaghayegh Ahmadzadeh-Asl

Received: 18 January 2010 / Accepted: 18 March 2010 / Published online: 8 April 2010

Abstract In this study, bioceramic nanocomposites were synthesized by sintering compacted bodies of hydroxyapatite (HA) mixed with 5 or 15 wt% nanosilicon carbide at 1100 or 1200°C in a reducing atmosphere. Pure hydroxyapatite was also prepared for comparison. Phase compositions, structural and physical properties of the composites were studied using appropriate techniques. Some in vitro biological properties of the composites were also investigated by using newrat calvaria osteoblastic cells. X-ray diffraction analysis indicated that tricalcium phosphate (TCP) comprising negligible α-TCP and considerable β-TCP were formed in composites during sintering meanwhile hydroxyapatite and silicon carbide (SiC) were also existed in the composition. Based on the results, that composite made of 5 wt% nanosilicon carbide exhibited higher bending strength, fracture toughness and bulk density than pure HA and composite with 15 wt% silicon carbide. The scanning electron microscopy coupled with energy dispersive X-ray analysis revealed that the addition of nanosilicon carbide suppressed the grain growth and yielded a feature of island-type clusters consisting of blistered calcium phosphate (HA and TCP) and SiC grains. Also, in this study, better proliferation rate and alkaline phosphatase activity were observed for the osteoblastic cells seeded on top of the composites compared to pure HA. Overall, the results indicated that the composite of 95 wt% hydroxyapatite and 5 wt% SiC exhibited better mechanical and biological properties than pure HA and further addition of SiC failed strength and toughness.

S. Hesaraki (✉) · T. Ebadzadeh
Department of Ceramics, Materials and Energy Research Center, Tehran, Iran
e-mail: s-hesaraki@merc.ac.ir

S. Ahmadzadeh-Asl
Department of Chemistry, Amirkabir University of Technology, Tehran, Iran

1 Introduction

The use of some bioceramics, such as tricalcium phosphate (TCP) and hydroxyapatite (HA) in the field of biomedical application has been developed in over the last three decades [1]. HA is interesting material for both dentistry and orthopedic applications because it forms a real bond with the surrounding bone and produces an osteointegrative tissue. Nevertheless, HA is mechanically poor and thus cannot be used as implant devices for stress-bearing applications [2].

Several studies have been performed to improve mechanical properties of HA by using sintering additives for consolidation of this material during heating.

Various types of additives including $CaCl_2$, KCl, KH_2PO_4, $(KPO_3)_n$, $Na_2Si_2O_5$, K_2CO_3, Na_2CO_3, KF, sodium phosphates and other compounds based on P_2O_5–CaO system have been considered by Suchanek et al. [3] as sintering aids. Takami and Kondo [4] described various P_2O_5–CaO based frit-form additives for sintering HA. The phase transformation and mechanical properties of composites of HA and P_2O_5–CaO frits (10–50 wt%) were also described [5, 6]. Georgiou and Knowles [7] used additives from the ternary Na_2O–P_2O_5–CaO system for the same purpose. Hu et al. also reported the use of a borosilicate glass up to 50 wt% as HA sintering additive [8].

However, it is well known that the mechanical properties can also be improved by incorporation of a reinforcing phase such as fibers, whiskers, platelets or particles into the ceramic matrix. In the case of biocompatible ceramics, the additive should either be present in natural bones or belong to the group of bioinert materials.

Silicon carbide (SiC) is a well known ceramic material with excellent physical properties such as high resistance to chemicals, excellent thermal/heat conductivity and superior mechanical properties. SiC has been widely studied as a dense material for preparation of composite materials [9–12]. Especially, the preparation of nano-sized silicon carbide has received considerable attention, because it allows the preparation of bulk materials with increased plasticity [10] or nanocomposites with enhanced mechanical and tribological properties [13]. The use of nanosilicon carbide for reinforcement of ceramics such as alumina has been reported in literatures [14].

There are numbers studies that reported use of silicon carbide for different clinical purposes. It has been indicated that SiC and hydroxyapatite are equally biocompatible materials for clinical studies [15]. The possible use of silicon carbide (SiC) as a ceramic coating material for titanium-based total hip replacement (THR) implants was studied by Santavirta et al. [16]. They stated that SiC was a promising ceramic for total hip replacement (THR) implant coating, because it reduced wear debris formation from the soft titanium surface.

Amorphous silicon carbide (a-SiC) films, deposited by plasma-enhanced chemical vapor deposition was also evaluated as insulating coatings for implantable microelectrodes and biocompatibility of SiC was proved by implantation of SiC-coated quartz discs in the subcutaneous space of the New Zealand rabbits [17].

This study was performed to assess the effect of adding nanosilicon carbide to HA on structural, physical, mechanical and biological properties of obtained composites. The role of sintering temperature on the above mentioned properties was also investigated.

2 Materials and methods

2.1 Starting materials

Starting materials used in this study were commercial HA (Merck, 2196) and nanosilicon carbide (Plasmachem, R 36/37/38 S 26).

Particle size distribution of HA powder was measured by laser particle sizer analyzer (Fritsch analysette 22) in an aqueous medium. Particle size of nanosized SiC was recorded by using the zeta sizer and its particle morphology was observed using transmission electron microscopy (TEM) technique as follows: The SiC powder was ultrasonically dispersed in ethanol to form a diluted suspension and then a few droplets were dropped on carbon coated-copper grids. The morphology of the particles was observed by TEM instrument (GM200 PEG Philips) which operated at an accelerating voltage of 200 kV.

Since wet method would be selected for homogenizing SiC and HA, stable suspension of HA should be prepared at a proper pH condition. Thus, the influence of pH on zeta potential (ZP) of HA was investigated by using a zeta sizer device (Zetasizer 300HS). Hydrochloric acid and ammonia solution were used to provide acidic and alkaline pH of the suspension, respectively.

2.2 Preparation of HA–nanosilicon carbide mixture

Different formulations of HA–SiC composites were investigated, pure HA without any SiC (H100), mixture of 95 wt% HA and 5 wt% SiC (H95S5) and mixture of 85 wt% HA and 15 wt% SiC (H85S15). To mix the composite components (HA and SiC) the following procedure was used: An aqueous suspension of HA and nanosized SiC was prepared at 25°C and pH was adjusted to 10 using ammonium hydroxide solution. Then, the solvent phase was evaporated while the suspension was stirring on top of a heater. Both heating and stirring processes were simultaneously continued until a paste was achieved. The paste was then transferred to an oven and dried at 105°C for 24 h until a homogenized powder was obtained.

2.3 Thermal treatment for preparation of HA–SiC composites

For producing composites, the homogenized powder was poured into a cuboid-shaped steel mould and compressed at 20 bar pressure by uniaxial hydraulic press. The final dimension of specimens was $20 \times 5 \times 5$ mm^3. No binder was used in the pressing process. The compacted samples were sintered at 1100 and 1200°C in an electrical furnace in reducing atmosphere for two hours. Pure HA bodied was also prepared using the same processing condition for comparison.

3 Characterization of composites

3.1 Phase analysis

Phase composition of sintered samples was evaluated by using an automated X-ray diffractometer device (XRD, Philips PW3710). Cu-K_α radiation was adapted at operating condition of 40 kV and 30 mA and XRD data were collected over 2θ range of 10–20°.

3.2 Microstructure observation

Microstructure analysis of samples was performed by using scanning electron microscope (Stereoscan S 360-Leica Cambridge, England). Due to poor electrical conductivity

of the samples a thin layer of gold were coated on their surfaces before testing.

3.3 Mechanical properties

Cuboid-shaped specimens ($20 \times 5 \times 5$ mm^3) were prepared as described in Sect. 2.3. Bending strength (σ) was recorded in triple point mode by using a universal mechanical testing device (Instron IV 1196). A crosshead speed of 1 mm/min was used and σ value was calculated using the following expression:

$$\sigma = \frac{3Pl}{2bd^2} \tag{1}$$

where P was load of fracture (in N), b, l and d were width, length and thickness of the sample (in mm), respectively. Five samples of each composition were tested for statistical purposes.

The indentation method was employed to measure toughness and hardness of the samples. The surface of the samples were polished by using sandpaper (up to 1200 number) and diamond paste (1, 3 and 6 μm) and then, an indent was created on the sample surface by using a Vickers indentor (MVK-C11, Akashi, Japan) at 200 g force for 15 s. After 30 s, fracture toughness of the specimens (K_{IC}) was estimated according to the Lawn and Fuller formula:

$$K_{IC} = 0.0726\,\frac{P}{3C^{\frac{3}{2}}} \tag{2}$$

where P was indentation load and C was average length of cracks. For measuring hardness, various loads of 2.94, 4.90 and 9.81 (N) were exerted at loading time of 10 s using MVH-H21 indentation device (Akashi, Japan). Additionally, the hardness (H) was calculated by the following equation:

$$H = \frac{P}{2a^2} \tag{3}$$

where P was the applied load (in N) and a was the average diameter of the formed indent.

3.4 Density and porosity measurements

Bulk density (D_b) and total porosity (P_t) of the sintered samples were recorded using the following expressions:

$$D_b = \frac{m}{v} \tag{4}$$

$$p_t = 100\left(1 - \frac{D_b}{D_{t-c}}\right) \tag{5}$$

where m was weight of specimen, V was its volume and D_{t-c} was theoretical density of sintered sample (pure HA or HA–SiC composite). To calculate D_{t-c}, firstly, the phase composition of each specimen was determined quantitatively by using the following equation [18]:

$$X_a = \frac{I_{(hkl)\alpha}}{RIR_\alpha I^{rel}_{(hkl)\alpha}} \left[\frac{1}{\sum_{j=1}^{\#phase} \left(I_{(hkl)'j}/RIR_j I^{rel}_{(hkl)'j}\right)} \right], \tag{6}$$

where α was the phase to be determined, X_α was weight fraction of α phase, j was another phase or phases existed in the composition. $I_{(hkl)\alpha}$ and $I_{(hkl)j}$ were, respectively, intensity of hkl peaks of α and j phase in XRD patterns and the $I^{rel}_{(hkl)}$ term ratios the relative intensities of the peaks used. If the maximum (100%) peaks of all phases (e.g. α and j) are used, the value of this term is 1. RIR_α or RIR_j which is I_α/I_c or I_j/I_c ratio can be extracted using inorganic crystal structure database (ICSD). ICSD provides this ratio for all phases using corundum (Al_2O_3) as standard samples. Note that the sum of all fractions of all phases must be 1 [for more details see Ref. 17]. In this study, the following ICSD collection codes were used: ICSD # 034457 for HA, ICSD # 006191 for β-TCP and ICSD # 015325 for SiC.

Regarding the theoretical density of hydroxyapatite (3.16 g/cm^3), silicon carbide (3.21 g/cm^3) and beta-tricalcium phosphate (3.06 g/cm^3), the main components of specimens, D_{t-c} of the sintered specimens was calculated by using rule of mixture:

$$D_{t-c} = \sum_{\alpha=1}^{n} v_\alpha D_{t-\alpha} \tag{7}$$

where D_{t-c} was theoretical density of specimen, $D_{t-\alpha}$ was theoretical density of i constituent of the composite and v_α was volume fraction of α in composite which can be calculated regarding its density and weight percentage in composite.

3.5 Biological evaluations

Biological properties of the specimens were evaluated using osteoblastic cells derived from newborn rat calvaria. The cells were isolated by sequential collagenase digestion from calvaria of newborn (2–5 days) Wistar and cultured in Dulbecco modified Eagle medium (DMEM; Gibco-BRL, Life Technologies, Grand Island, NY) supplemented with 15% fetal bovine serum (FBS; Dainippon Pharmaceutical, Osaka, Japan) and 100 g/ml penicillin–streptomycin (Gibco-BRL, Life Technologies) in 5% CO_2 and 95% air atmosphere at 37°C for 1 week. The medium was changed every 2 days. The confluent cells were dissociated with trypsin and subcultured to 3 passages which were used for tests.

The disc-shaped pure HA or HA/nanosilicon carbide composite specimens (6 mm in diameter and 3 mm in height) were sterilized using 70% ethanol and the

osteoblastic cells were seeded onto the tops of the glass discs at 2×10^3 cells/disc. Polystyrene discs with diameter of 6 mm (the same surface area compared to glass specimens) were prepared from the tissue culture plate and similarly were seeded with the cells as control specimens. The specimen/cell constructs were placed into 24-wells culture plates and left undisturbed in an incubator for 3 h to allow the cells to attach to them and then an additional 3 ml of culture medium was added into each well. The cell/specimen constructs were cultured in a humidified incubator at 37°C with 95% air and 5% CO_2 for 2, 5, and 7 days. The medium was changed every 3 days.

The proliferation of the osteoblastic cells on top of the specimens was determined using the MTT (3-{4,5-dimethylthiazol-2yl}-2,5-diphenyl-2H-tetrazolium bromide) assay. For this purpose, at the end of each evaluating period, the medium was removed and 2 ml of MTT solution was added to each well. Following incubation at 37°C for 4 h in a fully humidified atmosphere at 5% CO_2 in air, MTT was taken up by active cells and reduced in the mitochondria to insoluble purple formazan granules. Subsequently, the medium was discarded and the precipitated formazan was dissolved in dimethylsulfoxide, DMSO, (150 ml/well), and optical density of the solution was read using a microplate spectrophotometer (BIO-TEK Elx 800, Highland Park, USA) at a wavelength of 570 nm.

To observe the morphologies of the cells attached onto the surfaces of the pure HA (H100), H95S5 and H85S15 specimens, the cells were cultured onto the discs as described above. After 7 days, the culture medium was removed, the cell-cultured specimens were rinsed with phosphate buffered saline (PBS) twice and then the cells were fixed with 500 ml/well of 3% glutaraldehyde solution (diluted from 50% glutaraldehyde solution (Electron Microscopy Science, USA) with PBS). After 30 min, they were rinsed again and kept in PBS at 4°C. Specimens were then fixed with 1% Osmium tetroxide (Polyscience, Warmington, PA, USA). After cell fixation, the specimens were dehydrated in ethanol solutions of varying concentration (30, 50, 70, 90, and 100%) for about 20 min at each concentration. The specimens were then dried in air, coated with gold and analyzed by SEM (Streoscan S 360, Cambridge).

The osteoblastic cells were also seeded on the disc specimens under the same culturing conditions as described above to determine the level of ALP produced by them on days 2, 5 and 7. Cells were rinsed twice with phosphatase buffered saline (PBS) followed by trypsinization and then scraped into double-distilled water. The cell lysates were frozen and thawed three times to disrupt the cell membranes. ALP activity was measured at 405 nm using *p*-nitrophenyl phosphate (pNPP) (Sigma, USA) as the substrate. A 50 ml sample was mixed with 50 ml pNPP (1 mg/ml) in 1 M diethanolamine buffer containing 0.5 mM $MgCl_2$, pH 9.8 and incubated at 37°C for 30 min on a bench shaker. The reaction was stopped by the addition of 50 ml of 1 N NaOH. Total protein content was determined using Coomassie brilliant blue method as described elsewhere [19].

4 Statistical analysis

Data were processed using Microsoft Excel 2003 software and the results were produced as mean ± standard deviation of at least 4 experiments. Significance between the mean values was calculated using standard software program (SPSS GmbH, Munich, Germany) and the $p \leq 0.05$ was considered significant.

5 Results and discussion

5.1 Characteristics of starting materials

Average particle size of SiC (d_{mean}) measured by zeta sizer was 80 nm. Figure 1 shows TEM image of SiC particles used as starting material in this work. Spherical particles are observed with diameter up to 100 nm.

Another starting material, i.e. HA exhibited a d_{mean} value of 0.9 μm in alkaline aqueous solution. It is suggested that this value relates to the aggregated particles. This suggestion is confirmed by the SEM micrograph of sintered HA samples (which are shown in Sect. 3.3) where their grain size is lower than 500 nm. Determination of zeta potential value against pH changes relates to stability of HA suspension. Note that no dispersing agent was used for stabilizing HA suspension. ZP correlates to particle surface charge and it can determine the stability of

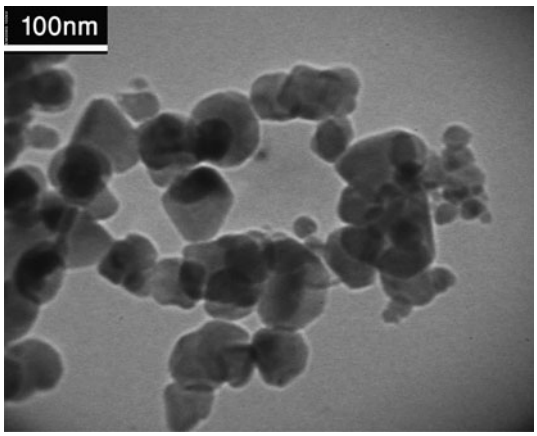

Fig. 1 TEM image of the nanosized silicon carbide used for fabrication of HA/SiC composites (*Scale bar* = 100 nm)

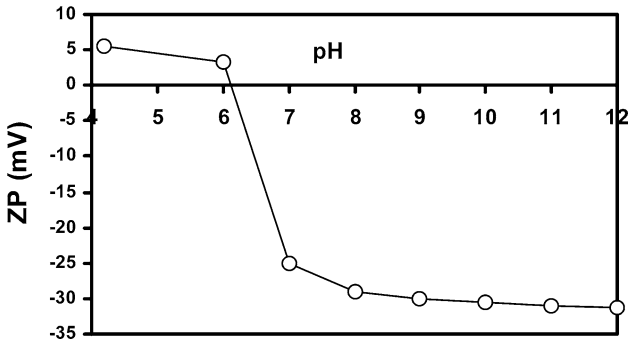

Fig. 2 Zeta potential of HA particles as a function of pH

suspension by preventing particle association due to repulsive forces between them. Figure 2 shows changes of ZP as a function of suspension pH. ZP value decreases with increasing pH until it reaches to an approximately constant value at pH >8. In this study it was necessary to perform the homogenizing process at pH values much higher than isoelectric point of SiC particles, thus it was performed at pH = 10.

5.2 Phase analysis

Figure 3 shows X ray diffraction patterns of different samples sintered at 1100°C (Fig. 3a) and 1200°C (Fig. 3b) for 2 h. For H100, the only existed phase for both sintering temperatures of 1100 and 1200°C is HA (ICSD # 034457). Thus these sintering temperatures have no influence on its phase composition. In H95S5 and H85S15 samples sintered at 1100°C, in addition to HA, other calcium Phosphate phases including β-TCP (ICSD # 006191) and slight amount of α-TCP (ICDD # 29-359) are also observed. Note that in H95S5 β-TCP is a predominant phase (at both 1100 and 1200°C), whereas in H85S15 HA is dominant. Silicon carbide can be protected from oxidation by using reducing atmosphere and the silica-rich layer probably formed its surfaces. Thus, the initiated peak at $2\theta = 35.7$ relates to SiC (ICSD # 015325). The intensity of SiC peak is proportional to its concentration in the composites.

On the whole, it is obvious that samples which are produced by adding SiC to HA are biphasic compounds of HA and TCP or Si-doped TCP [20]. In samples with 5 wt% SiC, predominant phase is β-TCP for both temperatures whereas in samples with 15% SiC, HA is a dominant phase only at 1200°C. It should be regarded that XRD peaks of Si-doped TCP are too much similar to TCP peaks and it is difficult to recognize them. Some authors reported formation of TCP from HA at elevated temperatures (above 800°C), which is provoked by adding SiO_2 or bioglass additives [20]. The type and content of each phase depends on both additive concentration and sintering temperature. Regarding our results, it is confirmed that formation of TCP phases (β-TCP or α-TCP) is induced by adding silicon containing materials like SiC.

5.3 Microstructure

Microstructures taken from fractured surfaces of different samples with different sintering temperatures are shown in Fig. 4. Microstructure of HA sample at 1100°C consists of micropores and approximately spherical-shaped grains with relatively similar dimensions of 200–300 nm. Apatite sintering at 1200°C leads to initiation of grain growth due to formation of island shaped clusters beside micropores. The presence of micropores is suitable for attachment of osteoblastic cells.

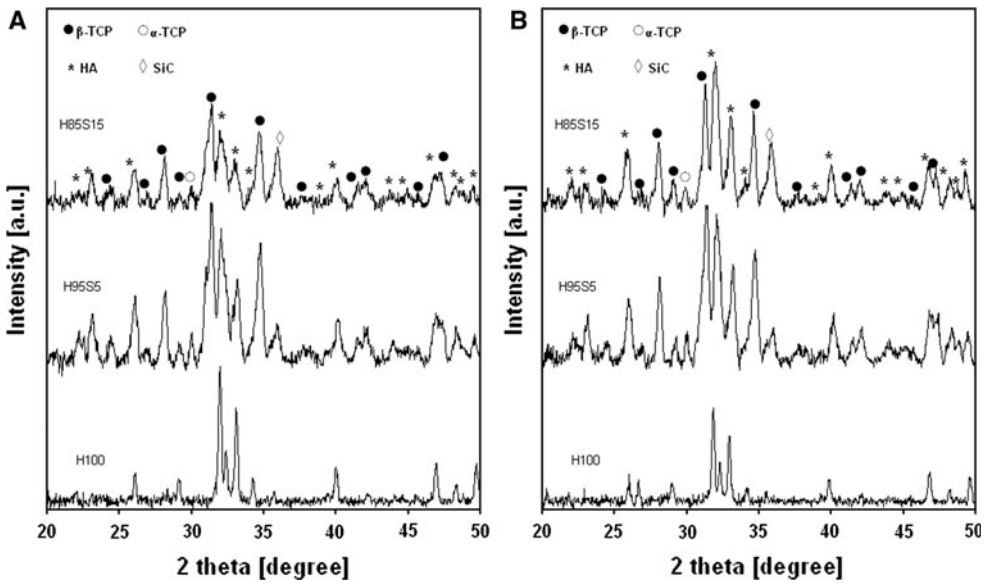

Fig. 3 XRD patterns of pure HA and HA–SiC composites sintered at different temperatures: **a** 1100°C and **b** 1200°C

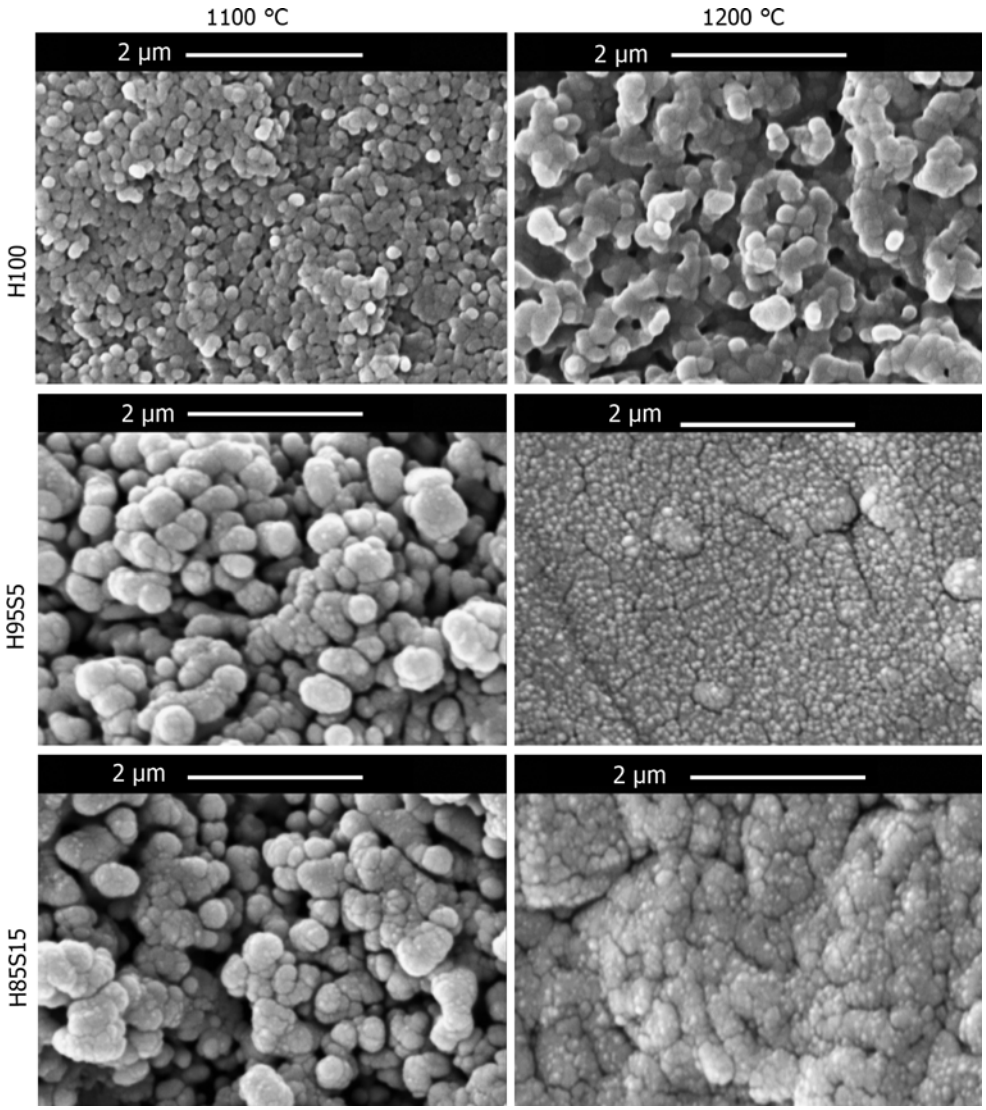

Fig. 4 SEM micrographs of pure HA and HA–SiC composites sintered at different temperatures (Scale bar = 2 μm)

Microstructures of SiC-containing composites are totally different. In both H95S5 and H85S15 specimens, clusters of raspberry shape particles are seen within a microporous matrix in which the contents of micropores decrease dramatically with increasing sintering temperature leading to formation of more compacted structure. The energy dispersive X-ray analysis (EDXA) patterns of the samples sintered at 1200°C (corresponded to SEM images in Fig. 4) are shown in Fig. 5. For HA specimen, Ca and P and for H95S5 and H85S15 composites Ca, P and Si are the major elements detected by this coupled technique. Regarding the size of the phases and the used magnification, it is not possible to extract the accrue analysis of a certain point in the SEM images, because the electron beam spot size is larger than the size of each phase and the found elements are resulted from a broad region in the irradiated electron beam area. Overall, regarding the EDXA data and XRD patterns of the samples, the microstructures of composites consist of both SiC and HA phases tightly connected together. Comparing SEM and EDXA patterns of H100 and H95S5 and H85S15 samples suggests that the blistered grains in microstructure of HA–SiC specimens are produced due to the presence of SiC nanoparticles. Nanosized SiC particles can exhibits improved sinterability due to their superior surface area. Formation of a SiO_2-rich layer on the surfaces of SiC particles due to their partial oxidation is also suggested. It can be found from the matrix that the SiC particles were uniformly distributed in the HA matrix. It should be noted that growth of HA grains is limited by the presence of SiC particles. It is major factor that behind enhanced mechanical properties of composite as will be mentioned in next section. It seems that volume of micropores in H85S15 is higher than that of H95S5. It is also confirmed quantitatively by the percentage of total porosity as shown in the next section.

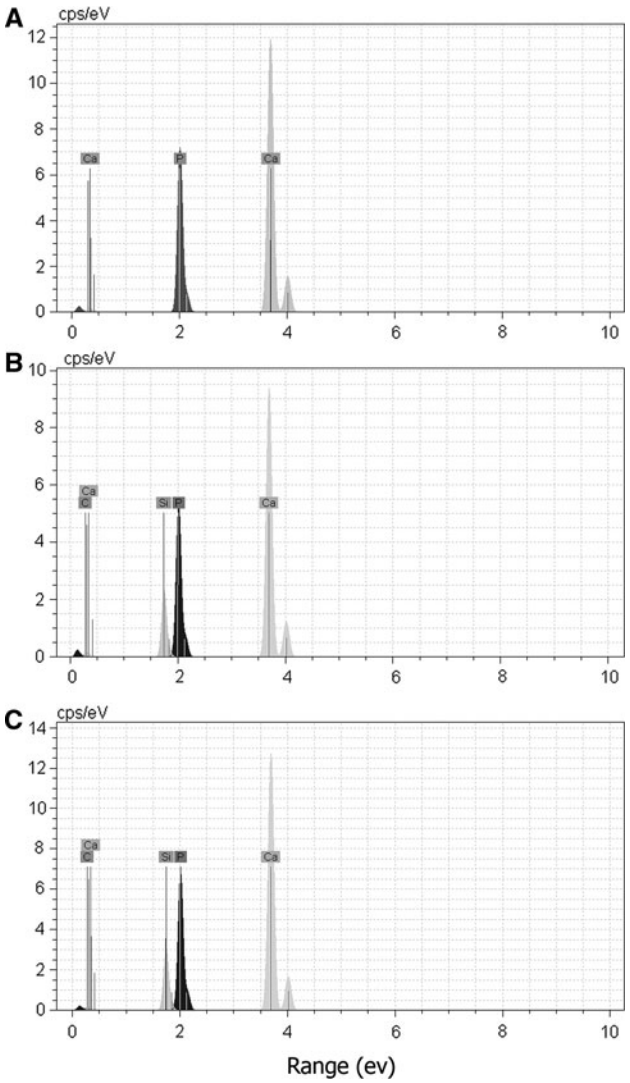

Fig. 5 EDXA patterns of **a** H100, **b** H95S5 and **c** H85S15 specimens corresponding to the SEM images of those samples sintered at 1200°C (Fig. 4)

5.4 Physical and mechanical properties

Table 1 shows some physical and mechanical properties of different studied composites. The maximum value of bending strength belongs to H95S5 and adding more than 5% of SiC causes decrease of σ. The bending strength increases with increasing sintering temperature too.

It is observed from Table 1 that fracture toughness (K_{IC}) increases with increasing sintering temperature; meanwhile the maximum K_{IC} value is reported for H95S5. The presence of SiC nanoparticles and their preventional role in crack propagation as well as fine-grain microstructure are responsible for increased toughness of this HA–SiC composite. There is a description for the increased fracture toughness of nanoSiC-containing composites such as TiC/SiC. It has been stated that when a crack progressed forward and reaches the SiC particles distributed at the boundaries of HA grains, it is difficult for the crack to cross through the SiC particles and the crack will be deflected and propagates along the matrix and SiC grains boundaries [21]. The similar statement can also be used to discuss improved K_{IC} of HA/SiC composites.

Increase in strength and toughness of other ceramics such as Al_2O_3 added by small amount of nanosized silicon carbide have been also reported [22, 23]. In addition to above mentioned descriptions, changes in mechanical strength of different samples can be explained by their measured porosities. It is observed that the total porosity increased by increasing temperature. Thus H95S5 sintered at 1200°C has minimum content of porosity. On the other hand, a reverse result is achieved for bulk density. The increased porosity of H85S15, a sample with considerable amount of SiC, probably is due to the partial decomposition of SiC to SiO_2 and CO_2. It is obvious that mechanical strength will be decreased with increasing porosity.

As shown in Table 1, the hardness value of HA increases by using 5 wt% of nanosized SiC in the composition. This issue is more obvious when samples are sintered at 1200°C. However, the change in H value of HA in not statistically significant by adding 15 wt% nanosized SiC. It is stated that the hardness of ceramic materials is strongly influenced by porosity [24]. Thus, the increased hardness of H95S5 may be related to its low porosity content. Substitution of SiC, a naturally hard material, for HA in the composition can be referred as another reason for this matter.

Table 1 Some physical and mechanical properties of HA and HA/SiC composites sintered at 1100 and 1200°C

		σ (MPa)	K_{IC} (MPa.m$^{0.5}$)	H (GPa)	D_b (g/cm^3)	P_t (%)
H100	1100	17.45 ± 2.33	0.55 ± 0.05	0.91 ± 0.10	2.24 ± 0.05	31.01 ± 4.30
	1200	26.65 ± 4.25	0.71 ± 0.04	2.56 ± 0.31	2.51 ± 0.04	19.13 ± 3.22
H95S5	1100	23.67 ± 3.46	0.69 ± 0.03	1.11 ± 0.09	2.26 ± 0.03	30.47 ± 4.51
	1200	39.80 ± 5.05	0.85 ± 0.03	3.07 ± 0.12	2.83 ± 0.03	12.76 ± 3.36
H85S15	1100	15.27 ± 4.33	0.52 ± 0.02	1.01 ± 0.21	2.29 ± 0.02	29.72 ± 2.55
	1200	23.94 ± 1.46	0.65 ± 0.04	2.47 ± 0.09	2.69 ± 0.11	17.16 ± 5.74

It is necessary to emphasize that the differences between the results of various studies which reported mechanical properties of HA invigorated with various additives/admixtures not only is due to diversity of reinforcing phase but also is resulted from differences in fabrication and testing procedures.

5.5 Cell response

Figure 6 shows the results of proliferation test measured for various specimens after different culturing periods. After cell seeding, the osteoblasts begin to proliferate in a time-dependent manner, because the difference in number of viable cells existed on top of the same specimens is statistically significant for different periods ($P < 0.05$). At 2nd day, no significant difference in cell proliferation is observed between the control (polystyrene) and other samples ($P \gg 0.05$). At 5th day, the amount of formazan produced by osteoblasts cultured on H100 is comparable to that of polystyrene ($P < 0.05$), while better proliferation is observed for H95S5 and H85S15. The same result is also observed for the samples at 7th day.

Figure 7 that shows the morphologies of the osteoblastic cells attached onto the surface of the glass specimens can confirm the results of MTT assay. In all samples, the surface has been covered by polygonal osteoblastic cells with developed cytoplasmic extensions and the cells became confluence on top of the composites after 7 days. Note to the higher abundance of osteoblasts on SiC-containing composites in comparison with pure HA.

Alkaline phosphatase is known as an early osteoblastic differentiation marker [25] produced by cells showing mineralized extracellular matrix. ALP activity (Fig. 8) is increased from 2nd day to 5th day of culture ($P < 0.01$) for all samples and then inhibited on 7th day for H95S5 and H85S15 specimens ($P < 0.05$), probably due to conflux of expanded cells. At day 5th, higher lever of ALP is observed for HA/SiC composites compared with both pure HA and control sample ($P < 0.05$). There is no significant difference in ALP activity of osteoblasts on H100 and composites at 7th day ($P > 0.05$).

Overall, the results of cell culture tests express better biological performance of SiC-containing HA in comparison with the pure HA. It is suggested that is due to the production of a Si-containing material when combining SiC with HA. The surprising effect of Si ions on proliferation and activity of osteoblasts have been well documented in literatures [26].

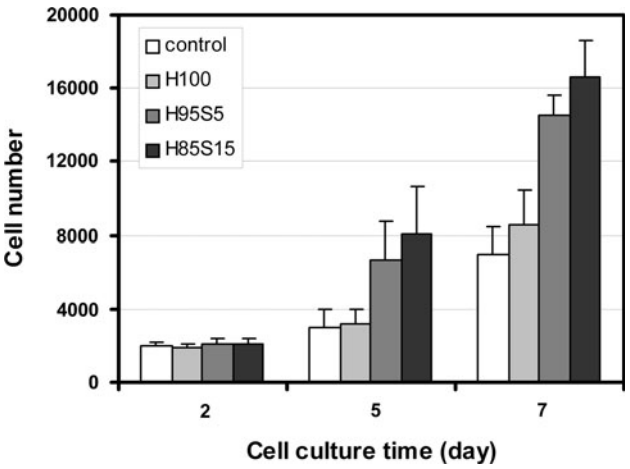

Fig. 6 Proliferation of rat calvaria osteoblasts on the surfaces of various HA-based composites studied in this work

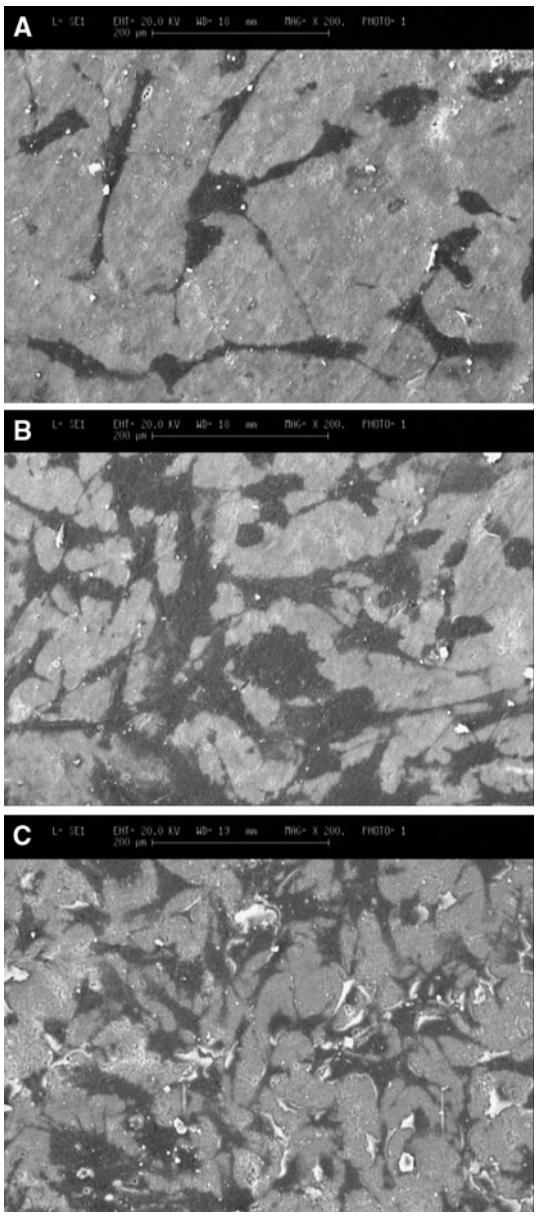

Fig. 7 SEM morphology of the osteoblasts cultured on the surfaces of specimens for 7 days: **a** H100, **b** H95S5 and **c** H85S15

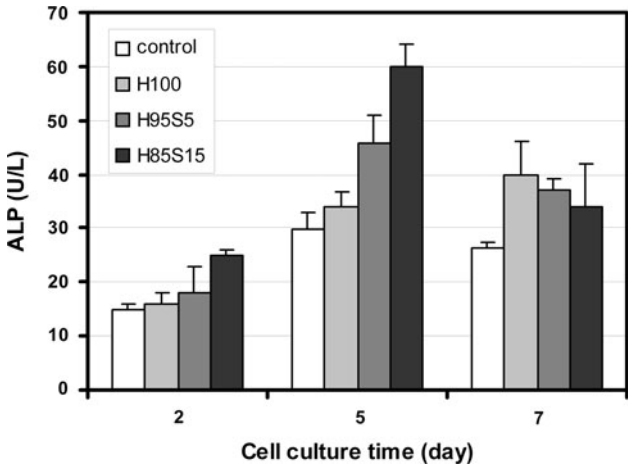

Fig. 8 ALP activity of the osteoblastic cells seeded on the surfaces of various samples as a function of culture time

6 Conclusions

The following conclusion can be resulted from this study:

(1) Phase composition of HA–SiC composites depends on different parameters such as sintering temperature and amount of each component, whereas in pure HA, phase composition is independent of sintering temperature.
(2) Both porosity and bending strength of SiC-HA composites depend on concentration of SiC so that these properties are improved by adding 5% SiC to HA and fail by increasing SiC content up to 15%.
(3) The addition of SiC suppresses grain growth of calcium phosphate phases during sintering.
(4) SiC can enhance proliferation rate and alkaline phosphatase activity of osteoblastic cells when it is added to HA to provide HA–SiC composite.

Acknowledgements The authors gratefully acknowledge Materials and Energy Research Center for financial supports and Ms. Gholami and Mr. Nasiri for their assistance in this work.

References

1. Liu DM, Chou HM. Formation of a new bioactive glassceramic. J Mater Sci Mater Med. 1994;5:7–10.
2. Kalita SJ, Bose S, Hosick HL, Bandyopadhyay A. CaO–P_2O_5–Na_2O-based sintering additives for hydroxyapatite (HAp) ceramics. Biomaterials. 2004;25:2331–39.
3. Suchanek W, Yashima M, Kakihana M, Yoshimura M. Hydroxyapatite ceramics with selected sintering additives. Biomaterials. 1997;18:923–33.
4. Takami A, Kondo K. Phosphate of calcium ceramics. US Patent 4,308,064, 1983.
5. Safina MN, Safronova TV, Lukin ES. Calcium phosphate based ceramic with a resorbable phase and low sintering temperature. Glass Ceram. 2007;64:19–24.
6. Tancred DC, McCormack BAO, Carr AJ. A quantitative study of sintering and mechanical properties of hydroxyapatite/phosphate glass composites. Biomaterials. 1998;19:1735–43.
7. Georgiou G, Knowles JC. Glass reinforced hydroxyapatite for hard tissue surgery: part 1. Mechanical properties. Biomaterials. 2001;22:2811–5.
8. Hu Y, Miao X. Comparison of hydroxyapatite ceramics and hydroxyapatite/borosilicate glass composites prepared by slip casting. Ceram Int. 2004;30:1787–91.
9. Raczka M, Gorny G, Stobierski L, Rozniatowski K. Effect of carbon content on the microstructure and properties of silicon carbide-based sinters. Mater Character. 2001;46:245–9.
10. Stobierski L, Gubernat A. Sintering of silicon carbideI. Effect of carbon. Ceram Int. 2003;29:287–92.
11. Ibrahim IA, Mohamed FA, Lavernia EJ. Particulate reinforced metal matrix composites—a review. J Mater Sci. 1991;26:1137–56.
12. Rajan TPD, Pillai RM, Pai BC. Reinforcement coatings and interfaces in aluminium metal matrix composites. J Mater Sci. 1998;33:3491–503.
13. Sternitzke M. Structural ceramic nanocomposites. J Eur Ceram Soc. 1997;17:1061–82.
14. Gustafsson S, Falk LKL, Liden E, Carlstrom E. Alumina/silicon carbide composites fabricated via in situ synthesis of nano-sized SiC particles. Ceram Inter. 2009;35:1293–6.
15. Coletti C, Jaroszeski MJ, Pallaoro A, Hoff AM, Iannotta S, Saddow SE. Biocompatibility and wettability of crystalline SiC and Si surfaces. Conf Proc IEEE Eng Med Biol Soc. 2007;5850–3.
16. Santavirta S, Takagi M, Nordsletten L, Anttila A, Lappalainen R, Konttinen YT. Biocompatibility of silicon carbide in colony formation test in vitro. A promising new ceramic THR implant coating material. Arch Orthop Trauma Surg. 1998;118:89–91.
17. Cogan SF, Edell DJ, Guzelian AA, Ping Liu Y, Edell R. Plasma-enhanced chemical vapor deposited silicon carbide as an implantable dielectric coating. J Biomed Mater Res A. 2003;67:856–67.
18. Chung FH. Quantitative interpretation of X-ray diffraction patters. I. Matrix-flushing method of quantitative multicomponent analysis. J Appl Crystallogr. 1974;7:519–25.
19. Neuhoff V, Stamm R, Eibl H. Clear background and highly sensitive protein staining with coomassie blue dyes in polyacrylamide gels: a systematic analysis. Electrophoresis. 1985;6:427–48.
20. Reid JW, Pietak A, Sayer M, Dunfield D, Smith TG. Phase formation and evolution in the silicon substituted tricalcium phosphate/apatite system. Biomaterials. 2005;26:2887–97.
21. Wang L, Jiang W, Chen L. Fabrication and characterization of nano-SiC particles reinforced TiC/SiCnano composites. Mater Let. 2004;58:1401–4.
22. Borsa CE, Jones NMR, Brook RJ, Todd RI. Influence of processing on the microstructural development and flexure strength of Al2O3/SiC nanocomposites. J Eur Ceram Soc. 1997;17:865–72.
23. Sciti D, Vicens J, Bellosi A. Microstructure and properties of alumina–SiC nanocomposites prepared from ultrafine powders. J Mater Sci. 2002;37:3747–58.
24. Timothy P, Hoepfner ED. Case. The influence of the microstructure on the hardness of sintered hydroxyapatite. Ceram Int. 2003;29:699–706.
25. Elgendy HM, Norman ME, Keaton AR, Laurencin CT. Osteolike cell (MC3T3–E1) proliferation on biorodible polymers: an approach towards the development of a bone-bioerodible polymer composite material. Biomaterials. 1993;14:263–9.
26. Pietak AM, Reid JW, Stott MJ, Sayer M. Silicon substitution in the calcium phosphate bioceramics. Biomaterials. 2007;28:4023–32.